

# Understanding B-type supergiants in the low metallicity environment of the SMC II.

C. Trundle<sup>1,2</sup> & D.J. Lennon<sup>1</sup>

<sup>1</sup> The Isaac Newton Group of Telescopes, Apartado de Correos 321, E-38700, Santa Cruz de La Palma, Canary Islands, Spain

<sup>2</sup> The Department of Pure and Applied Physics, The Queen's University of Belfast, Belfast BT7 1NN, Northern Ireland

**Abstract.** Despite a resurgence of effort over the last decade in the area of massive stars there is still ambiguity over their evolutionary path, contamination of their surface abundances and the behaviour of their stellar winds. Here 10 SMC B-type supergiants are analysed applying a unified model atmosphere code FASTWIND to intermediate resolution spectra from the ESO Multi Mode Instrument (EMMI) on the NTT telescope. Combined with the 8 targets analysed in paper 1 (Trundle *et al.* 2004), this work provides observational results on the properties of the winds and chemical compositions of B-type supergiants in the SMC. This paper emphasizes and substantiates the implications for stellar evolution from paper 1; that current theoretical models need to produce larger degrees of surface nitrogen enhancements at lower rotational velocities. In addition a significant discrepancy between theoretical and observed mass-loss rates is discussed which will have important implications for the rotational velocities obtained from stellar evolution calculations. Furthermore, an initial calibration of the wind-momentum luminosity relationship for B-type supergiants in a low metallicity environment ( $Z = 0.004$ ) is presented.

**Key words.** stars: atmospheres – stars: early-type – stars: supergiants – stars: mass-loss – stars: abundances – stars: evolution

## 1. Introduction

The evolution of a galaxy is strongly influenced by the input of energy, momentum and processed material from massive stars into the interstellar medium (ISM). As possible progenitors of Type II supernovae and gamma ray bursts, the nucleosynthesis processes and evolution of massive stars are important topics in current astrophysical research. In spite of its importance, there is still a large degree of ambiguity concerning the evolutionary path of these objects beyond the main-sequence and the influence of rotation and mass-loss on the composition of their stellar photospheres. Hence quantitative observational studies concerning the chemical compositions and winds of massive stars are vital tests on both the theory of galactic and stellar evolution. These early-type stars are also important contributors to the spectra of star-forming galaxies and intermediate age (20-50 Myr) stellar populations (de Mello *et al.* 2000). Furthermore in order to model the integrated light of starburst regions and constrain the composition of high redshift galaxies, accurate atmospheric and wind parameters of OB stars are required (Leitherer *et al.* 1999; Pettini *et al.* 2000).

In the mid 1990's an intriguing implication arose from the theory of radiatively driven winds and was introduced by

Kudritzki, Lennon & Puls (1995). This work showed that the wind-momentum of a star, a product of its mass-loss, terminal velocity and radius, is directly related to its luminosity and can therefore provide an estimate of the stellar distance. The intrinsically high luminosity of early-type supergiants coupled with their relatively normal spectral behaviour makes them the best candidates for using this Wind-momentum Luminosity Relationship (WLR). Recent work has shown the dependence of the WLR on spectral type for Galactic OBA-type stars (Puls *et al.* 1996; Kudritzki *et al.* 1999; Repolust, Puls & Herrero 2004; Markova *et al.* 2004). Some studies have also endeavoured to understand the behaviour of the WLR in the lower metallicity environments of the Magellanic Clouds (Puls *et al.* 1996; Kudritzki & Puls 2000; Crowther *et al.* 2002; Trundle *et al.* 2004; Evans *et al.* 2004a). Most of these studies focused on relatively small samples of O-type stars with some indication of the WLR having different behaviour at lower metallicity. Recent work by Trundle *et al.* (2004; hereafter paper 1) investigated a sample of B-type supergiants in the SMC. Although the sample only included 8 targets, it provided observational evidence to test line driven wind theory in this spectral region and at a low metallicity. Indeed this work highlighted a significant discrepancy between the observed mass-loss rates and the theoretical predictions by Vink *et al.* (2001) at SMC metallicities.

In addition to wind analyses, Paper 1 investigated the chemical composition of the SMC sample. This provided quantitative CNO abundances of B-type supergiants; a key test of the mixing and mass-loss processes incorporated in stellar evolution models for early-type stars. The results from Paper 1 are

Send offprint requests to: C.Trundle at ctrundle@ll.iac.es.

Recently moved to Instituto de Astrofísica de Canarias, C/ Vía Láctea, E-38200 La Laguna Tenerife, Spain.

**Table 1.** Observational details. Identification numbers are from Azzopardi & Vignean (1982; AV#) and Sanduleak (1968; Sk#). Spectral types adopted from Lennon (1997), except for AV78 which has been reclassified in this work from the blue spectra. Absolute Magnitudes ( $M_v$ ) are calculated using V and (B-V) magnitudes from Garmany, Conti & Massey (1987;<sup>1</sup>) and Massey (2002;<sup>2</sup>) and (B-V)<sub>0</sub> values from Fitzpatrick & Garmany (1990). The adopted distance modulus is 18.9 (Harries, Hilditch, & Howarth 2003). The average S/N ratios for the blue and red arms are presented. The  $v \sin i$  values represent the width of the spectral features and are simply upper limits on the projected rotational velocities (see Paper 1).

STAR	Alias	Spectral Type	V	B - V	$M_v$	S/N		$v_{lsr}$ (kms <sup>-1</sup> )	$v_{\sin i}$ (kms <sup>-1</sup> )
						B	R		
AV420	Sk131	B0.5 Ia	13.09 <sup>2</sup>	-0.17	-5.90	84	49	188 ± 12	80
AV242	Sk85	B1 Ia	12.11 <sup>1</sup>	-0.13	-6.91	125	47	188 ± 25	90
AV264	Sk94	B1 Ia	12.36 <sup>1</sup>	-0.15	-6.60	102	74	142 ± 14	85
AV78	Sk40	B1 Ia <sup>+</sup>	11.05 <sup>1</sup>	-0.03	-8.25	161	80	176 ± 12	85
AV96	Sk46	B1.5 Ia	12.59 <sup>2</sup>	-0.10	-6.50	146	69	161 ± 10	90
AV373	Sk119	B2 Ia	12.17 <sup>1</sup>	-0.09	-6.92	80	105	191 ± 26	80
AV10	Sk7	B2.5 Ia	12.58 <sup>2</sup>	-0.02	-6.69	80	110	225 ± 21	85
AV56	Sk31	B2.5 Ia	11.15 <sup>1</sup>	-0.00	-8.18	120	100	209 ± 11	80
AV443	Sk137	B2.5 Ia	10.97 <sup>1</sup>	-0.06	-8.18	165	160	191 ± 22	73
AV151	Sk57	B2.5 Ia	12.26 <sup>2</sup>	-0.02	-7.01	122	80	187 ± 15	62

consistent with the significant enhancements and dispersions of nitrogen abundances, previously observed in B-type stars (Gies & Lambert 1992; Lennon et al. 1991, 1996, 1997, 2003; Fitzpatrick & Bohannan 1993; McErlean, Lennon, & Dufton 1999; Dufton et al. 2000). The existence of a stellar wind can reduce the angular momentum of a star, which in turn causes a decrease in the rotational velocity. This link between the mass-loss of a star and its rotational velocity affects the stellar lifetimes and photospheric composition predicted by stellar evolution codes. Thus mass-loss rates, rotational velocities and abundances are important observational constraints for such codes. The recent inclusion of rotationally induced mixing in stellar evolution codes such as those by Maeder & Meynet (2001), were shown in paper 1 to reproduce the large dispersion of nitrogen abundances observed in B-type supergiants, implying that rotation may play a significant role in the evolution of massive stars.

The dataset of Lennon (1997) offers the opportunity of analysing an additional ten B-type supergiants which supplements the results from paper 1 and will provide a clearer insight into the behaviour of these luminous objects. The objective of this work is to provide observational constraints on the mass-loss rates of B-type supergiants and to calibrate the WLR at the metallicity of the SMC.

## 2. Observational Data

The SMC optical dataset considered for this work is a subset of that presented by Lennon (1997), in a study to delineate the spectral classifications of B-type supergiants in low metallicity environments. The medium resolution spectra ( $R \sim 20000$ ) were obtained remotely on the NTT telescope with the ESO Multi Mode Instrument (EMMI). Three spectral regions were observed covering the wavelengths 3925-4375 Å, 6190-6830 Å and 4300-4750 Å. Signal-to-noise (S/N) ratios greater than 70 were obtained along with dispersions of 0.45 and 0.32 Å

per pixel in the blue and red arms, respectively (see Table 1). Further details of the observations and data reduction procedures can be found in Lennon (1997).

The original data selected by Lennon (1997) are a subset of B0 - B9 stars from the sample of Garmany *et al.* (1987), who carried out a spectral classification of SMC OB-type stars. For the purpose of this paper ten stars from this dataset have been selected spanning the spectral range B0 - B2.5. An additional constraint was that each object have medium to strong stellar winds, which was apparent from the profile of the H<sub>α</sub> line. In Table 1 the targets are listed with the spectral types assigned by Lennon (1997) from applying his revised classifications for B-type supergiants in the SMC. AV78 has been reclassified here as a B1 Ia<sup>+</sup> star due to the presence of a weak Si IV line in its spectrum at 4116 Å. This star was previously classed as a B1.5 Ia<sup>+</sup> star by Lennon (1997).

The estimated projected rotational velocities ( $v \sin i$ ) were determined using the techniques described in paper 1 and are presented in Table 1. It is important to note that the  $v \sin i$  values only represent the width of the spectral features and are simply upper limits for the projected rotational velocities (*i.e.* no attempt has been made to deconvolve the contribution of stellar rotation and macroturbulent motions from the line broadening). Equivalent widths were measured by fitting a Gaussian profile using a non-linear least squares technique in DIPSO (Howarth et al. 2003); a spectrum analysis package from STARLINK. Table 1 also lists the absolute magnitudes calculated using V and (B-V) magnitudes from Garmany, Conti & Massey (1987) and Massey (2002) and (B-V)<sub>0</sub> values from Fitzpatrick & Garmany (1990). The adopted distance modulus of the SMC, applied to determine the absolute magnitude ( $M_v$ ), is 18.9 (Harries, Hilditch, & Howarth 2003).

Radial velocities of the target stars are corrected to the local standard of rest, giving a range in velocities of 142 - 225 kms<sup>-1</sup> (note similar range observed for SMC stars in Paper 1). From a H I 21 cm emission survey by McGee & Newton (1981), four

gas complexes were identified in the SMC at heliocentric velocities of 114, 134, 167 & 192  $\text{kms}^{-1}$ . In addition Welty *et al.* (1997) found SMC multiple absorption components of interstellar gas with velocities between  $85 \leq$  and  $210 \text{ kms}^{-1}$ . This implies that the radial velocities of our target stars are consistent with those of field stars in the SMC.

### 3. Stellar parameters

The model atmospheres and procedures used in this analysis are identical to those described in Paper 1 and will only briefly be repeated here. The ‘unified model atmosphere’ code applied is called FASTWIND, a line-blanketed, spherically symmetric, non-LTE code (Santolaya-Rey, Puls, & Herrero (1997); Herrero, Puls, & Najarro 2002; Repolust, Puls, & Herrero 2004). The temperature structure in FASTWIND was not calculated explicitly, but parameterised by applying the non-LTE Hopf function described by Santolaya-Rey, Puls, & Herrero (1997; see equations 4.1 - 4.3) to TLUSTY models calculated at Queen’s University Belfast (Ryans, R.S.I.; private communication).

The stellar parameters were calculated using precisely the same methods as described in Paper 1. In short, the parameter space in which each star resides was estimated using a coarse grid and this was followed by an iterative process to determine each parameter accurately in a finer but smaller grid. The resulting photospheric and wind parameters for each target are presented in Table 2.

For the B0.5 - B2 stars, effective temperatures were determined from the Si III/Si IV ionisation balance with typical random errors of 1.5 kK. In the B2 - B2.5 stars only the Si III lines were present, as a result profile fitting to these lines was required to determine the temperature. For these objects, the lack of a Si IV 4116 Å line and the very weak features for the Si II 4128, 4131 Å profiles acted as upper and lower limits for the temperature estimates. The only exception to this is AV151 which exhibited relatively strong Si II features allowing the Si II/Si III ionisation balance to be determined. The uncertainty for AV151 is 1.5 kK, and is slightly larger for the other B2-B2.5 stars (2.0 kK). This uncertainty in effective temperature also affects the determination of the logarithmic surface gravity, typically an error of 0.5 kK represents a systematic error of 0.05 dex in  $\log g$ . In addition to this there is a random error of  $\pm 0.05$  for the B2-B2.5 stars and up to 0.1 dex for the B0-B1.5 stars (See Table 2).

Microturbulent velocities,  $\xi_{\text{Si}}$ , adopted for the analysis were derived from the Si III triplet at 4560 Å. The microturbulence was also derived from the O II multiplets, in the stars with spectral type earlier than B2. As discussed in paper 1 these values tend to be  $\sim 10 \text{ kms}^{-1}$  higher than estimated from the silicon lines. In the case of the stars cooler than B2, no O II lines are present in the spectra as a result of the low temperatures and hence low ionisation of this species. For AV56 the spread in equivalent widths amongst the Si III multiplet was only  $\sim 50 \text{ mÅ}$  and this was not sufficient to provide an accurate microturbulent velocity (typically this spread is  $> 100 \text{ mÅ}$  in the rest of the sample). In addition AV56 is too cool for it to have a well developed O II spectrum, preventing an estimation

of  $\xi_{\text{O}}$  and therefore a value of  $10 \text{ kms}^{-1}$  was adopted in the analysis for this star.

Three targets, AV242, AV264 & AV78, were included in the UV analysis of Evans *et al.* (2004 - hereafter EVANS04) (described in Paper 1), using archive IUE/HIRES data for AV78 and HST/GHRS spectra for the former two stars. These objects, therefore have predetermined terminal velocities measured with the SEI (Sobolev Exact Integration) method from the UV resonance lines. The remaining seven stars have no available UV data from which terminal velocities can be measured and hence estimates were made using the alternative procedure described in Paper 1 & EVANS04. This involves calculating the escape velocity and applying the ratios of  $v_{\infty}/v_{\text{esc}}$  determined by Kudritzki & Puls (2000) (viz. for  $T_{\text{eff}} \geq 21 \text{ kK}$  this ratio is equal to 2.65 and for  $T_{\text{eff}} < 21 \text{ kK}$  it is 1.4).

$H_{\alpha}$  profiles provide a means to determine the properties of the stellar wind; with a knowledge of the terminal velocity, the mass-loss rate ( $\dot{M}$ ) and beta parameter ( $\beta$ ) can be determined simultaneously from the profile shape.  $\dot{M}$  controls the overall wind emission in the profile, whilst  $\beta$  causes a variation in the strength and FWHM of the emission peak. As such it is difficult to constrain the beta parameter in stars with weak winds, where wind emission may only cause a small amount of filling in of the absorption core (viz. AV420; see Fig 1). In fact a variation of  $\beta$  from 0.8 to 2 for AV420 with subsequent changes in  $\dot{M}$  from  $0.49$  to  $0.14 \cdot 10^{-6} M_{\odot} \text{ yr}^{-1}$  will reproduce the observed  $H_{\alpha}$  profile. In this analysis we adopt a  $\beta$  parameter of 1 for this weak wind star with the knowledge that this will lead to uncertain mass-loss rates (see also AV216 and AV104 in Paper 1).

For the P-Cygni and emission profiles,  $\beta$  can be determined rather more accurately on the order of  $\pm 0.5$ . This is considerably higher than the error found from the UVES data and is attributed to the lower resolution and in some cases lower S/N of the current dataset. In addition, nebular contributions in AV96 & AV264 prevent accurate estimates of the emission peak FWHM and a  $\beta$  in the range 2 - 3 can generally fit these profiles with values above 3 having little impact on the profile shape. Since  $\dot{M}$  and  $\beta$  are derived simultaneously from the fitting of  $H_{\alpha}$  the error in the mass-loss rate is dominated by this uncertainty in  $\beta$ . The difference in  $\dot{M}$  derived with a  $\beta$  of 2 and of 3 is  $\sim 25\%$ . In the case of AV264 a value of 3 was deemed more appropriate from a fit to the redward wing of the emission profile and the height of the emission peak.  $\beta$  parameters for AV373 & AV151 are as uncertain as that for AV96 due to the failures in the code to produce complete emission profiles at low temperatures (see below) and which contribute to the error in the mass-loss rate derived. Uncertainties in the mass-loss rates therefore range from 15% to 25% and are presented in Table 2.

The final model fits to the observed  $H_{\alpha}$  profiles are presented in Figs. 1. Three of the objects, AV78, AV443 & AV56 display strong broadening in their profile wings (similar to AV362 & AV22 in paper 1). These wings, which are formed in the upper layers of the photosphere, are considerably affected by incoherent electron scattering. The introduction of electron scattering into the formal solution of the FASTWIND models provides an excellent profile fit to AV78 (B1Ia<sup>+</sup>; see Fig. 1).

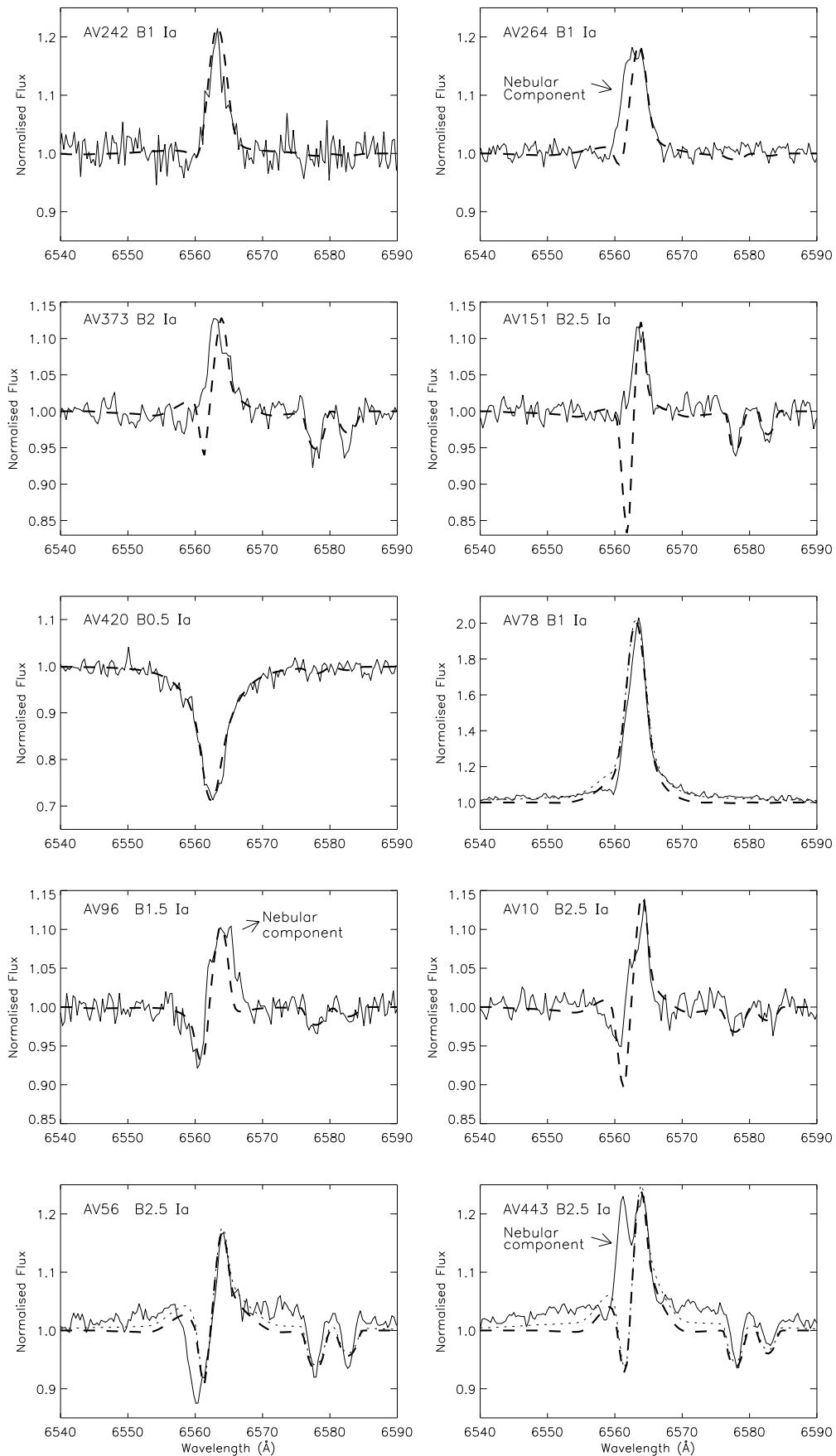


**Fig. 1.**  $H_\alpha$  profiles for the ten SMC B-type supergiants. The solid-dashed lines (---) are the best fits from the FASTWIND models and the parameters are given in Table 2. In the case of AV78, AV56 & AV443, models with the best fit parameters but with incoherent electron scattering included in the formal solution are also shown (dotted line; ···).

**Table 2.** Derived atmospheric and wind parameters for SMC B-type supergiants. The microturbulence from both the Si III & O II lines are presented, however the silicon microturbulence was adopted in the analysis. A microturbulence of  $10 \text{ km s}^{-1}$  was adopted for AV56 due to lack of a direct method of measurement. Escape velocities are calculated using the procedure outlined in paper 1 & EVANS04. Terminal velocities, ( $v_\infty$ ), for AV242, AV264 & AV78 are derived from the SEI method (1). For the rest of the sample,  $v_\infty$  is calculated by adopting a  $\frac{v_\infty}{v_{\text{esc}}}$  ratio of 2.65 for stars with  $T_{\text{eff}} \geq 21.0 \text{ kK}$  and 1.40 for  $T_{\text{eff}} < 21.0 \text{ kK}$  (2). The errors quoted are discussed in Section 3.

Star	$T_{\text{eff}}$ (kK)	$\log g$ (cgs)	$R_*$ ( $R_\odot$ )	$M_{\text{spec}}$ ( $M_\odot$ )	$M_{\text{evol}}$ ( $M_\odot$ )	$\log(\frac{L_*}{L_\odot})$	$\xi_{\text{Si}}$ ( $\text{kms}^{-1}$ )	$\xi_{\text{O}}$ ( $\text{kms}^{-1}$ )	$\dot{M}$ ( $10^{-6} M_\odot \text{ yr}^{-1}$ )	$v_\infty$ ( $\text{kms}^{-1}$ )	$v_{\text{esc}}$ ( $\text{kms}^{-1}$ )	$\beta$	$\log(D_{\text{MOM}})$ (cgs)
AV420	$27.0 \pm 1.5$	$3.05 \pm 0.15$	21.7	19	26	5.35	13	25	$0.34 \pm 0.15$	$1310 \pm 260^2$	$493^2$	1.0	$28.11 \pm 0.40$
AV242	$25.0 \pm 1.5$	$2.85 \pm 0.15$	36.6	35	39.5	5.67	13	20	$0.84 \pm 0.13$	$950 \pm 100^1$	$359^1$	2.0	$28.48 \pm 0.15$
AV264	$22.5 \pm 1.5$	$2.55 \pm 0.15$	34.8	16	29	5.44	13	19	$0.29 \pm 0.06$	$600 \pm 100^1$	$313^1$	2.5	$27.81 \pm 0.20$
AV78	$21.5 \pm 1.5$	$2.40 \pm 0.15$	79.0	57	53	5.92	12	20	$2.29 \pm 0.34$	$450 \pm 50^1$	$423^1$	3.0	$28.76 \pm 0.15$
AV96	$22.0 \pm 1.5$	$2.55 \pm 0.15$	34.0	15	27	5.39	11	21	$0.24 \pm 0.06$	$850 \pm 170^2$	$320^2$	3.0	$27.87 \pm 0.25$
AV373	$19.0 \pm 2.0$	$2.30 \pm 0.20$	46.8	16	28	5.42	11	22	$0.16 \pm 0.04$	$390 \pm 80^2$	$282^2$	3.0	$27.42 \pm 0.25$
AV10	$17.0 \pm 2.0$	$2.20 \pm 0.20$	46.7	13	22	5.21	14		$0.15 \pm 0.03$	$380 \pm 75^2$	$273^2$	3.0	$27.39 \pm 0.20$
AV56	$16.5 \pm 2.0$	$2.05 \pm 0.20$	96.1	38	50	5.88	10		$0.51 \pm 0.08$	$420 \pm 85^2$	$302^2$	2.0	$28.12 \pm 0.15$
AV443	$16.5 \pm 2.0$	$1.95 \pm 0.20$	96.5	30	42	5.79	11		$0.45 \pm 0.09$	$340 \pm 70^2$	$246^2$	2.0	$27.97 \pm 0.20$
AV151	$16.0 \pm 1.5$	$2.10 \pm 0.15$	57.1	15	24	5.28	15		$0.16 \pm 0.04$	$370 \pm 85^2$	$263^2$	3.0	$27.45 \pm 0.25$

However it doesn't completely account for the strong wings observed in the two cooler B2.5Ia type stars; this was also the case for AV362 (B3Ia) & AV22 (B5Ia). Also note the models failure to reproduce the observed profiles for spectral types later than B2 Ia (typically for  $T_{\text{eff}}$  below 19kK). The models below these temperatures exhibit strong absorption features not present in the observed spectra. In these models, the Lyman continuum is optically thick causing the transition from the 1<sup>st</sup> to 2<sup>nd</sup> energy levels to be in detailed balance and the second energy level then simulates a ground state. The  $H_{\alpha}$  line (*i.e.* transition from the 2<sup>nd</sup> to 3<sup>rd</sup> energy level) will subsequently result in a P-Cygni profile as it behaves like a quasi-resonance line. This may, in part, be due to the current temperature structures used in the FASTWIND models and could possibly be improved with the introduction of a temperature correction scheme. A new version of FASTWIND has recently been released which amongst other advances incorporates such a scheme (Puls *et al.* 2005). It is based on an alternative method introduced by Kubát, Puls & Pauldrach (1999) to solve the radiative equilibrium equation explicitly. With this technique, the temperature in the upper photosphere and wind is calculated by ensuring that a thermal balance of electrons is obtained.

One noticeable factor from Table 2 is the large values of the  $\beta$ -parameter determined for these B-type objects. These differ from those observed and predicted for O-type stars which have much faster winds with  $\beta$  being close to the order of unity. Indeed large  $\beta$  values have been observed in other optically based spectroscopic studies of B-type supergiants in the Galaxy and SMC (Kudritzki *et al.* 1999; Evans *et al.* 2004a). On the otherhand applying the SEI-method to UV P-Cygni lines of the SMC targets presented here and in Paper 1 and of the Galactic targets analysed in Kudritzki *et al.* suggest lower values of  $\beta$  of 1-1.5 (EVANS04 and Haser 1995, respectively). In both these UV analyses it was suggested that whilst small changes of  $\beta$  can give aesthetically more pleasing fits to the UV resonance lines, they were relatively insensitive to the parameter. In fact, Haser (1995) found that the SEI method of the B-type stars produce identical profiles for  $\beta$  values in the range 1-4. It is likely that the relatively slow winds of these objects result in the P-Cygni lines under sampling the velocity of the wind over the small range in depth for which the formation of these lines cover, in comparison to the  $H_{\alpha}$  profile. Hence the  $\beta$  parameter is ill defined by the UV lines in these slower wind objects.

#### 4. Chemical Composition

The procedures for the abundance analysis are identical to that discussed in Paper 1, they apply the same atmospheric models and atomic data and as such one would expect the abundances to follow the same patterns. Indeed, no surprises are hidden in the chemical composition of these 10 B-type supergiants. Consequently, a few interesting points will be introduced here with further discussions of the implications in the following section.

From a grid of equivalent widths generated by FASTWIND models at various microturbulent velocities and abundances, the absolute abundances of C, N, O, Mg & Si for the SMC stars were derived and are presented in Table 3. The dominant

uncertainties in these abundances are the adopted microturbulence,  $\xi_{Si}$ , equivalent widths and atomic data. In addition the lower resolution of the EMMI data causes a slight *relative* increase in the uncertainty of the equivalent width measurements, particularly for closely spaced, weak lines which may have been resolved in the UVES data but are slightly blended in the EMMI data (*viz.* Si IV 4116 Å & He I 4121 Å).

One difference in this work and that carried out for the UVES data are the number of nitrogen and oxygen lines considered in the abundance analysis. Experience with the B-type supergiant spectra identified some additional, reliable lines to be included in the analysis (*viz.* O II 4069, 4349 & 4676 and N II 4241 Å). In general the weakest lines in the UVES abundance analysis were not measurable in the EMMI data and were omitted from the analysis.

Following the procedures laid out in Paper 1, the carbon abundance was corrected for NLTE effects due to the problematic line 4267 Å. Table 3 states a mean carbon abundance of 6.89 dex, by applying the appropriate correction of +0.34 dex a mean C abundance of 7.23 dex is estimated for this sample.

It is worth noting, that preliminary abundance estimates for 64 SMC B-type supergiants were made by Dufton *et al.* (2000) in a study of line strengths (this work used the complete atlas of Lennon 1997). The Mg and Si results are in close agreement with those found here, whilst the C, N and O abundances, although lower differ by no more than 0.21 dex (see Table 4). Dufton *et al.* found a range of nitrogen abundances from 7.09 to 7.69 dex to fit the data, whilst the maximum value is smaller than that derived from the more detailed analysis in this work there is some consistency between the spread in results from the two analyses. This work shows that with a large sample, even basic analysis techniques can arrive at reasonable estimates for the chemical compositions of a stellar population.

#### 5. Discussion

For a comparison of our derived absolute abundances with the results of previous studies in the SMC, we will assume that the H II region abundances of Kurt *et al.* (1999) represent the present day composition of the SMC. In addition we include the results of Rolleston *et al.* (2003; corrected for non-LTE effects as discussed in Paper 1) for the main-sequence B-star, AV304, whose photosphere appears to be uncontaminated by any by products of nuclear processes in the stellar core. Thus, it is assumed that the chemical make-up of these objects represent the initial baseline composition of the SMC (for more on this topic see paper 1). The mean element abundance for this sample is presented in Table 3, but for the purpose of further discussion the results from all 17 supergiants and 1 giant will be considered. Hence Table 4 presents the mean abundances calculated by combining the results in Table 3 and those presented in Table 5 of paper 1. The results from SMC A-type supergiants and other B-type stars are also included in Table 3 (Venn 1999; Venn & Przybilla 2003; Lennon, Dufton & Crowley 2003, these are corrected for non-LTE effects see Paper 1).

A close examination of Table 4 reveals that the  $\alpha$ -processed elements (O, Mg, & Si) are in agreement for all objects, with

**Table 3.** Derived non-LTE absolute abundances for SMC B-type supergiants. Abundances are given as  $\log [N(X)/N(H)] + 12$ , where X represents the element under consideration. The errors represent the standard deviation of the mean and account for systematic errors. The numbers in the parenthesis are the number of lines included in the analysis. Mean element abundances are presented in the final line of the table.

Star	C II	N II	O II	Mg II	Si II	Si III	Si IV
AV420	<7.08 (1)	$7.44 \pm 0.14$ (2)	$8.06 \pm 0.27$ (10)	$6.84 \pm 0.24$ (1)		$6.62 \pm 0.12$ (3)	$6.59 \pm 0.46$ (1)
AV242	<6.88 (1)	$7.40 \pm 0.19$ (1)	$8.24 \pm 0.27$ (8)	$6.84 \pm 0.38$ (1)		$6.87 \pm 0.10$ (3)	$6.91 \pm 0.30$ (1)
AV264	<6.61 (1)	$7.86 \pm 0.13$ (3)	$8.01 \pm 0.25$ (13)	$6.91 \pm 0.14$ (1)		$6.65 \pm 0.14$ (3)	$6.64 \pm 0.28$ (1)
AV78	<6.90 (1)	$8.30 \pm 0.24$ (7)	$7.86 \pm 0.16$ (12)	$6.95 \pm 0.16$ (1)		$7.22 \pm 0.11$ (3)	$7.26 \pm 0.45$ (1)
AV96	$6.88 \pm 0.22$ (3)	$7.67 \pm 0.23$ (8)	$8.09 \pm 0.22$ (13)	$6.97 \pm 0.25$ (1)		$6.85 \pm 0.21$ (3)	< 6.79 :(1)
AV373	$6.89 \pm 0.19$ (3)	$7.46 \pm 0.25$ (2)	$8.37 \pm 0.39$ (8)	$6.94 \pm 0.30$ (1)	<6.79 (2)	$6.74 \pm 0.15$ (3)	
AV10	$6.59 \pm 0.14$ (3)	$7.66 \pm 0.26$ (3)	$8.13 \pm 0.31$ (3)	$6.81 \pm 0.12$ (1)	<6.76 (2)	$6.69 \pm 0.16$ (3)	
AV56	$7.19 \pm 0.53$ (3)	$8.27 \pm 0.32$ (2)		$6.68 \pm 0.09$ (1)	<6.60 (2)	$6.64 \pm 0.22$ (3)	
AV443	$6.99 \pm 0.36$ (3)	$7.96 \pm 0.22$ (2)		$6.72 \pm 0.08$ (1)	<6.55 (2)	$6.63 \pm 0.18$ (3)	
AV151	$6.85 \pm 0.12$ (3)	$7.55 \pm 0.19$ (2)		$6.70 \pm 0.08$ (1)	$6.54 \pm 0.11$ (2)	$6.61 \pm 0.18$ (3)	
Mean	$6.89 \pm 0.18$	$7.76 \pm 0.28$	$8.11 \pm 0.16$	$6.84 \pm 0.11$	$6.65 \pm 0.12$	$6.75 \pm 0.18$	$6.84 \pm 0.27$

**Table 4.** Comparison of mean abundances for the complete SMC B-type supergiant sample (including results from paper 1) with previous studies of abundances in the SMC. Included are the mean abundances of A-type supergiants from Venn *et al.* (1999, 2003; Si corrected for non-LTE effects.), SMC main-sequence B-star AV304 (Rolleston *et al.* 2003; corrected for non-LTE effects), NGC330 cluster main-sequence B-stars (Lennon, Dufton & Crowley 2003; corrected for non-LTE effects) and SMC H II regions from Kurt *et al.* (1999). The numbers in italics represent the abundances predicted from EW measurements in SMC B-type supergiants by Dufton *et al.* (2000; D00).

	Supergiants			B stars		HII
	This work	<i>D00</i>	A-type	NGC330	AV304	regions
C	$7.27 \pm 0.14$	<i>7.10</i>		$7.26 \pm 0.15$	$7.41 \pm 0.18$	$7.53 \pm 0.06$
N	$7.71 \pm 0.32$	<i>7.49</i>	$7.52 \pm 0.10$	$7.51 \pm 0.18$	$6.55 \pm 0.01$	$6.59 \pm 0.08$
O	$8.13 \pm 0.13$	<i>7.95</i>	$8.14 \pm 0.06$	$7.98 \pm 0.13$	$8.16 \pm 0.33$	$8.05 \pm 0.05$
Mg	$6.81 \pm 0.14$	<i>6.78</i>	$6.83 \pm 0.08$	$6.59 \pm 0.14$	6.73	
Si	$6.75 \pm 0.18$	<i>6.78</i>	$6.92 \pm 0.15$	$6.58 \pm 0.32$	$6.74 \pm 0.03$	$6.70 \pm 0.20$

the possible exception of the NGC330 stars. The abundances of the  $\alpha$ -processed elements in the NGC330 stars appear to be lower than the other SMC objects by  $\leq 0.25$  dex. This cluster was found to be 0.5 dex metal deficient with respect to SMC field stars in a photometric study made by Grebel & Richtler (1992). However the results here concur with the lower metal deficiency of this cluster observed in recent analyses by Hill (1999) and Lennon, Dufton & Crowley (2004) on K and B-type stars, respectively. CN processed material is once again evident in the atmospheres of the B-type stars, the nitrogen abundances in the overall sample studied here varies from 7.14 dex in the giant, AV216, to 8.30 dex in the most luminous object in the sample, AV78. The lowest nitrogen enhancement in the supergiant sample is a factor of 7 (7.40 dex) above the nitrogen abundance of AV304 and the nebular results. This enrichment is in close agreement with the results from the A-type supergiants and B-type main-sequence stars (Venn 1999; Venn & Przybilla 2003; Lennon, Dufton, & Crowley 2003).

To understand the distribution of nitrogen abundances in OBA-type stars in the SMC, a histogram was assembled from the results in the literature (see Fig 2). In addition to the

results from the present study, the plot includes the abundances derived for OBA-type stars by Venn (1999), Crowther *et al.* (2002), Lennon, Dufton, & Crowley (2003), Hillier *et al.* (2003), Venn & Przybilla (2003) & Bouret *et al.* (2003). The histogram clearly illustrates that there is a large range in nitrogen abundances observed in these stars. The majority of the objects have enhanced abundances, which predominantly lie around  $\sim 7.50$  dex, closer to the baseline galactic nitrogen abundance than that of the SMC. The stars considered have stellar masses in the range 11 to 60  $M_{\odot}$ , thus to decipher any correlation with mass and subsequently luminosity the results for the 25  $M_{\odot}$  (box outlined in bold dashed line) and 40  $M_{\odot}$  (shaded box) OB stars have been over plotted in Fig 2 (no abundances for A stars in this mass range are available in the literature). Whilst there appears to be a trend of nitrogen abundance with mass, in that higher nitrogen abundances are produced in the most massive stars, it is unwise to make such definitive conclusions from the poor statistics available to us at present.

Recall that the signature of photospheric contamination by CN-cycled material is an enhancement in nitrogen with some depletion of carbon and possibly oxygen. No obvious sign of

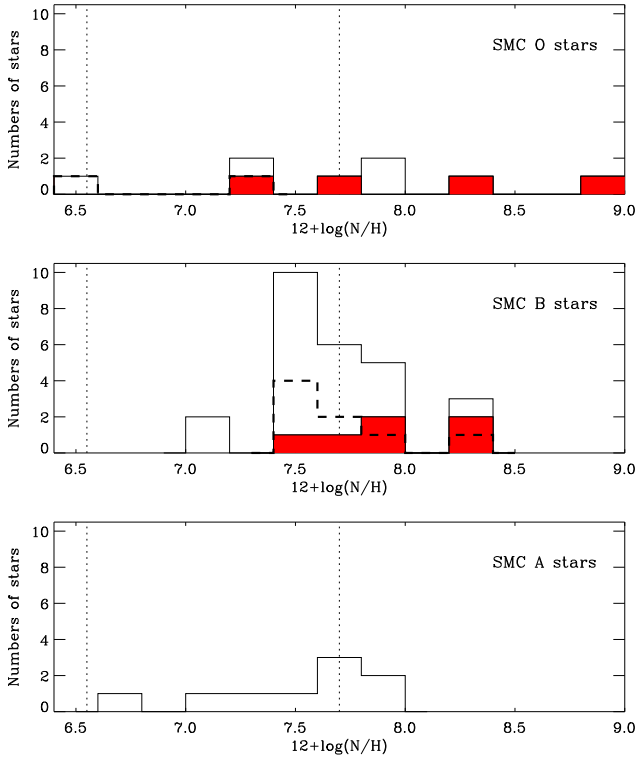


**Fig. 2.** Histogram of results from abundance analyses of SMC OBA-type stars collected from the literature. The dotted lines represent the baseline nitrogen abundances in the SMC (6.55 dex) and Milky Way (7.70 dex). The top panel shows the nitrogen abundance of O-type stars in the SMC using the results of supergiants of Crowther *et al.* (2002) and Hillier *et al.* (2003) and SMC O-type dwarfs of Bouret *et al.* (2003). The middle panel illustrates the distribution of observed nitrogen abundances from B-stars in the SMC, these include the results from this work and the B-type stars of Lennon, Dufton & Crowley (2003). The bottom panel includes the nitrogen abundance results of the A-type supergiants in the SMC from the analysis of Venn *et al.* (1999) with the updated values from Venn & Przybilla (2003). In the top and middle panel the distribution of stars with  $M_{\text{evol}} \sim 25 M_{\odot}$  (box outlined in bold dashed lines) and  $40 M_{\odot}$  (shaded box) from the original set of targets are also indicated.

depletions in oxygen have been detected in this sample of 18 stars, consistent with theoretical predictions that indicate moderate depletions in oxygen, smaller than the errors in our analysis. It is interesting to note that AV215 and AV78 (which have the highest N enhancements of 26 and 56 times the baseline value, respectively), have the lowest oxygen abundances, but these values are still within the error on the mean. In addition, the mean carbon abundance of the B-type supergiant sample and the NGC330 stars, are lower than that of AV304 and the H II regions, whether this is a significant difference is difficult to ascertain given the uncertainties in the absolute abundances of this ion. Within the B-type supergiant sample there is no evidence that AV216, (the giant and hence the least processed),

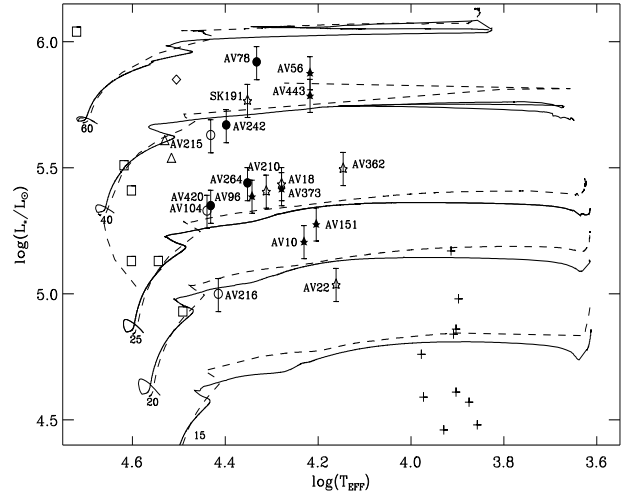


**Fig. 3.** HR-diagram, luminosity as a function of temperature. The stellar evolution tracks of Maeder & Meynet (2001) are shown for an assumed initial rotational velocity of 0 (—; solid lines) and  $300 \text{ km s}^{-1}$  (- -; dashed lines) at solar masses of 15, 20, 25, 40, &  $60 M_{\odot}$ . Included are the results from the early and mid B-type supergiants of both the UVES ( $\circ$  &  $\star$ ) and EMMI ( $\bullet$  &  $\star$ ) data, with errors in luminosity representing  $\pm 15\%$ . In addition, the SMC O-type supergiants of Hillier *et al.* ( $\triangle$ ; 2003) and Crowther *et al.* ( $\diamond$ ; 2002), SMC O-type dwarfs of Bouret *et al.* (open square; 2003) and AF-type supergiants from Venn *et al.* (+; 1999, updated by 2003) are also shown.

has a higher carbon abundance than the rest of the sample, nor that AV215 and AV78 have depleted carbon.

### 5.1. Evolution of B-type Supergiants

In paper 1 it was shown that stellar evolution models which include the effects of rotation can reproduce, for the most part, the observed nitrogen abundances in the SMC B-type stars. For the purpose of this discussion, the complete sample will again be compared to the evolution tracks of Maeder & Meynet (2001) which have been re-calibrated to a metallicity of  $0.2 Z_{\odot}$  (see Paper 1) and assume an initial rotational velocity of  $300 \text{ km s}^{-1}$ . The position of this stellar sample on the HR diagram is illustrated in Fig 3. From these tracks all of the stars seem to be past the end of the hydrogen burning main-sequence phase, with some of the objects having thick hydrogen burning shells. Indeed the loci of the cooler stars (B2.5 - B5) on the evolutionary tracks imply that they are in the core helium-burning phase.

In these comparisons one must be careful as the actual stars may have a range of initial rotational velocities rather than the  $300 \text{ km s}^{-1}$  assumed in the evolutionary models, and therefore the tracks presented in Fig 3 may be inappropriate for some, or all, of the stars. Including rotational velocities in the evolutionary models has the effect of extending the main-sequence branch to higher luminosities and to lower temperatures, which will therefore result in lower evolutionary masses for a star of a

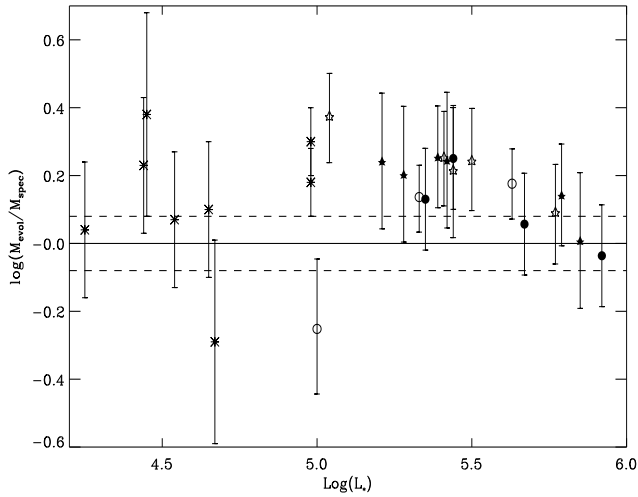


**Fig. 4.** Comparison of evolutionary and spectroscopic masses as a function of luminosity. Included are the results from the early and mid B-type supergiants of both the UVES ( $\circ$  & open star) and EMMI ( $\bullet$  &  $\star$ ) data. Additionally the results from NGC330 B-type stars from Lennon, Dufton & Crowley ( $\ast$ ; 2003) are shown. The error bars represent the error in the surface gravity. Also shown is the uncertainty in mass due to the adopted distance modulus (- -; dashed lines).

given luminosity. Stars with initial stellar masses  $> 15 M_{\odot}$  tend to cross the HR-diagram from the end of the main-sequence phase towards cooler temperatures with relatively constant luminosities, on the way to becoming red supergiants (RSG). Maeder & Meynet (2001) showed a comparison of evolutionary tracks adopting initial rotational velocities of 0, 200, 300 and  $400 \text{ km s}^{-1}$ , which implies only a small difference in luminosity ( $\Delta \log(L_{\odot}/L_{\star}) < 0.1$ ) as the star moves across the HR-diagram for an initial stellar mass of  $M_{\star} = 20 M_{\odot}$  (see Fig. 8 in Maeder & Meynet 2001). It is therefore reasonable to estimate evolutionary masses from these tracks, with the caveat that the assumed initial rotational velocities and the errors in interpolating between the tracks lead to uncertainties of  $\sim 5$  solar masses (and possibly more at the high end of the mass range under consideration).

The estimated evolutionary masses,  $M_{\text{evol}}$ , based on the  $300 \text{ km s}^{-1}$  tracks are displayed in Table 2 along with the spectroscopic masses,  $M_{\text{spec}}$ . These exhibit the same behaviour as found from the analysis of the UVES data, such that  $M_{\text{evol}} > M_{\text{spec}}$  by approximately 0.10 - 0.30 dex (see Fig. 4). The errors in the adopted distance and gravity account for much of the discrepancy, leaving only a difference of 0.10 dex (or  $\sim 8 M_{\odot}$ ). It is difficult to account for the remaining disagreement unless it is an overestimation of  $M_{\text{evol}}$  due to errors in interpolation. However, the largest discrepancies are observed in the less luminous, and hence less massive stars. In these stars the tracks are more widely spaced and therefore more accurate estimates of  $M_{\text{evol}}$  would be expected. By including some degree of convective overshooting the track for a given mass would be extended to higher luminosities and could account for at least

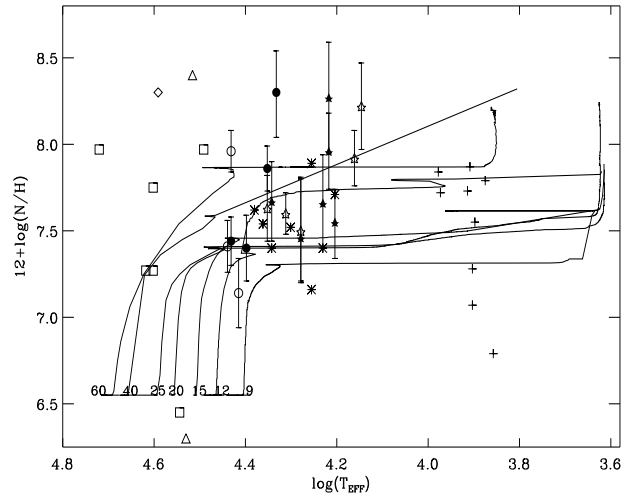


**Fig. 5.** Surface nitrogen abundances as a function of temperature. The stellar evolution tracks of Maeder & Meynet (2001) are shown for an assumed initial rotational velocity of  $300 \text{ km s}^{-1}$  and various solar masses. Included are the results from the early and mid B-type supergiants of both the UVES ( $\circ$  & open star) and EMMI ( $\bullet$  &  $\star$ ) data. Also displayed are the results from SMC O-type supergiants of Hillier *et al.* ( $\triangle$ ; 2003) and Crowther *et al.* ( $\diamond$ ; 2002), SMC O-type dwarfs of Bouret *et al.* (open square; 2003), NGC330 B-type stars of Lennon, Dufton, & Crowley ( $\ast$ ; 2003), and A-type supergiants from Venn *et al.* ( $+$ ; 1999, updated by 2003). The error bars illustrate the random and systematic errors on the nitrogen abundance.

some, if not all, of the overestimation in  $M_{\text{evol}}$ . Another possible explanation is that the lower luminosity stars may be in a post-RSG blue-loop phase and that the lifetime for this phase is greater than the pre-RSG stage.

To appreciate the success of the new evolutionary models, which consider rotation, in reproducing the observed nitrogen abundances in hot, luminous stars it is useful to look at the production of nitrogen as a function of temperature for various stellar masses (see Fig. 5). The models with stellar masses in the range  $20 - 60 M_{\odot}$  have nitrogen enrichments by the end of the core hydrogen burning phase of a factor of 7 to 20 above the baseline nitrogen abundance of 6.55 dex (from AV304). This is similar to the enhancements observed in our sample, although some of the more luminous objects have greater enhancements. Indeed, adopting a stellar mass for each object from the HR-diagram in Fig 3 and following the appropriate evolution track in Fig. 5, it would appear that many of the objects have greater enhancements than predicted. However given the errors in the abundance determinations this may not be significant. The two B2 Ia stars (AV373 & AV18) are interesting objects as they have very similar atmospheric and wind parameters, in addition their nitrogen abundances are the same, *within the errors*. This is also the case for the two B0.5 Ia stars, AV420 and AV104. Indeed the position of these four stars on the HR-diagram fall close to the theoretical predictions for a  $25 M_{\odot}$  star and have

abundances in agreement with the models for a  $25 M_{\odot}$  star with initial rotational velocities of  $300 \text{ km s}^{-1}$ .

From line driven wind theory, it is predicted that the stellar winds are stronger in stars of higher metallicity (*i.e.* that the mass-loss rates are higher). This comes directly from the dependence of the photon momentum transfer to the wind on the number of optically thick lines and that at lower metallicities the line strengths decrease. If this is the case, the loss of angular momentum by the end of the main-sequence is much greater in galactic objects than in lower metallicity stars (*viz.* SMC). This reduction in angular momentum at for example, solar metallicity, leads to a more rapid decrease in stellar rotational velocity. Therefore, the models by Maeder & Meynet (2001) for stars with  $Z = 0.004$  (SMC metallicity) have higher rotational velocities after core hydrogen burning than similar stars with solar metallicity. Since these stars have higher rotational velocities the convective zones are larger and the atmospheric distortions more severe, this results in greater enhancements in the nitrogen content of the photosphere.

*Do we observe this variation in rotational velocities from evolved stars in the two different environments?* Unfortunately this question is difficult to answer based on spectra alone. We do see greater nitrogen enrichments in the SMC stars, yet it is not possible to ascribe this to rotational velocities at present.  $v \sin i$  values have been measured for OBA-type stars in the galaxy and SMC but the estimates for both regions are similar (in the range  $40\text{-}150 \text{ km s}^{-1}$ ). However as noted previously in Sect. 2, these measurements are not truly representative of the projected rotational velocity but are dominated by macroturbulence. Also note that these are the projected rotational velocities and some information on the inclination of the rotational axis is required to enable the true velocity to be disentangled from  $v \sin i$  measurements.

## 5.2. Mass-loss: Observations and Predictions.

In this section the results of the entire sample of B-type supergiants will be discussed in an attempt to glean more information on the behaviour of their stellar winds as a function of luminosity, spectral type and metallicity. From a similar analysis of B-type stars in the Galaxy, Kudritzki *et al.* (1999) found a clear distinction between the wind momenta in early and mid B-type stars. This behaviour also differed from that of the O-type stars from Puls *et al.* (1996). This change in wind-momenta with spectral type is dependent on the flux weighted-distribution of the spectral lines, the ionisation of the lines contributing to the line force and the relative number of strong to weak lines driving the wind. The change in wind-momenta observed in B-type stars by Kudritzki *et al.* occurred between two objects with spectral types B1 and B1.5 at  $T_{\text{eff}} = 23.5$  and  $22.5 \text{ kK}$  (note these temperatures were determined from unblanketed models). This is approximately the point in which the so-called 'bistability jump', a change in the properties of the wind, is predicted to take place (Lamers, Snow & Lindholm 1995).

Due to the range in temperatures observed for the B1 stars in this sample and the fact that it overlaps with that of the B1.5

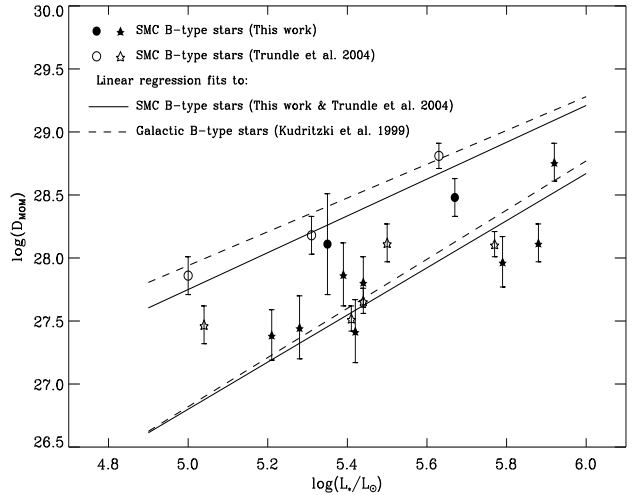


**Fig. 6.** WLR as derived from SMC B-type supergiants. The plot shows the early (circles) and mid (stars) B-type stars from the SMC sample (UVES: open symbols; EMMI: filled symbols). Included are the linear regression fits to the observational results of the early (all) and mid (only  $< B3$ ) B-type stars (—; solid lines). The dashed lines (---) are the wind-momentum-luminosity relationship, from galactic B-type supergiants without line-blanketing (Kudritzki *et al.* 1999). The error bars represent the uncertainty in deriving the wind momentum.

stars, it is more appropriate to make the early/mid B distinction based on stellar temperatures rather than spectral type. The hottest B1.5 star in this sample (Sk191) has an effective temperature of  $22.5 \text{ kK}$ . In Paper 1 it was shown that this object has a wind which behaves similar to the cooler stars, therefore this has been adopted as the cut off temperature for early B-type stars in the following discussion. This implies that AV264 and AV78 may exhibit signs of having lower wind momenta than the hotter B1 stars, but similar to that of the mid B-type stars. A direct comparison of the wind momenta for these stars with those of the hotter B1-type objects is not appropriate due to the luminosity dependence of the stellar wind.

No clear distinction between the wind-momenta of the SMC sample and the WLR of their galactic counterparts is evident. This consistency still holds if one regards the wind-momenta of the individual Galactic and SMC B-type supergiants at a certain luminosity, although a larger scatter is observed in the SMC mid B-type stars. It seems appropriate to attempt an estimation of the WLR from these SMC targets since they are the first homogeneous results from B-types stars in a low metallicity environment. We adopt the same form of the WLR as defined by Kudritzki *et al.* (1999)

$$\log D_{\text{mom}} = \log D_o + x \log(L_{\star}/L_{\odot}) \quad (1)$$

where the inverse of the slope,  $1/x = \alpha'$ .  $\alpha'$  describes the depth dependence of the radiative line force and can be expressed as a function of the force multiplier parameters of the radiative line force (*i.e.*  $\alpha' = \alpha - \delta$ ).  $D_{\text{mom}}$  is a product of the mass-loss

rate, terminal velocity of the wind and quadrature of the stellar radius.

The linear least squares fit to these results, which take into consideration the errors of both variables, can be seen in Fig 6 and the coefficients ( $\log(D_{\odot})$  and  $x$ ) are given in Table 5. The galactic WLR from Kudritzki *et al.* (1999) is also shown, however these did not include any uncertainty in luminosity which may taint the comparison with the SMC WLR. For the early B-type supergiants, the wind-momentum at a given luminosity is between 0.08 to 0.18 dex lower for the SMC stars than the Galactic stars. This difference is dependent on the luminosity due to the steeper slope of the SMC relationship. Theoretical and observational evidence suggests that stars with different luminosity classifications have wind momenta which vary (Puls *et al.* 1996; Puls, Springmann & Lennon 2000). Therefore it may be more appropriate to consider the WLR for only the four supergiants, omitting the giant AV216. The regression coefficients presented in Table 5 reveal that this results in a steeper WLR with  $\alpha' = 0.52$ , which is lower than that obtained from the Galactic B stars. However one must be cautious in interpreting these results as it is still a statistically poor sample.

The coefficients for the mid B-type stars are also included in Table 5. Considering all stars with  $T_{\text{eff}} < 22.5\text{kK}$ , results in a slightly shallower WLR than obtained for the Galactic stars. In paper 1 it was suggested that the cooler stars of the sample AV362 and AV22 (B3 and B5-type stars respectively) may exhibit a different behaviour to that of the mid B-types, possibly similar to that of the A-types. If this is the case then the mid B-type WLR should be determined only from those stars with  $22.5 > T_{\text{eff}} > 16\text{kK}$ . A steeper relationship is then obtained with  $\alpha' = 0.53$ , which is in very good agreement with the Galactic stars.

As mentioned earlier, Puls, Springmann & Lennon (2000) concluded from a theoretical study of the line forces driving the winds in massive stars that in lower density winds, lower  $\alpha$  and hence  $\alpha'$  exist. An interesting point is that this also suggests that a lower exponent is expected for low metallicity environments where the winds should be less dense, *i.e.* that  $\alpha'$  would be smaller at the metallicity of the SMC compared to stars with solar abundance. This is the case for the early-type stars but not for the mid B objects, yet the situation for the latter may be unclear as many of the Galactic objects are classed as Ib whilst those in the SMC sample are all more extreme type-Ia stars.

An additional effect to be considered in our interpretation of the results, is that the analysis carried out by Kudritzki *et al.* (1999) was based on unblanketed FASTWIND models. This results in lower wind-momenta than derived from blanketed models (see effect in Repolust, Puls, & Herrero 2004). Hence the true variation in wind-momenta will probably be found to be larger when compared to results from similar model atmosphere analyses. This may explain why no significant metallicity dependence is evident here. In order to investigate this, a preliminary Galactic WLR has been determined from two Galactic early B-type objects analysed by Urbaneja (2004) using a line blanketed version of FASTWIND. Indeed from Fig 7 a significant difference of  $\sim 0.5$  dex is observed between this relationship and that derived from the SMC objects. Although this is only derived from two objects, it supports the theoret-

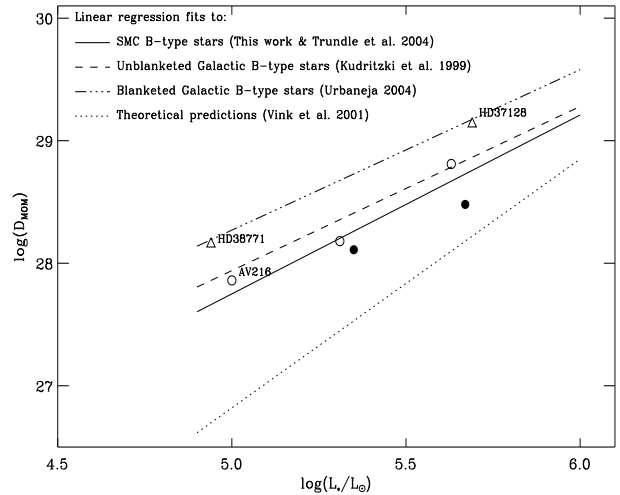


**Fig. 7.** Calibration of WLR with metallicity for SMC early B-type supergiants. The plot shows linear regression fits to the early B-type stars from the SMC sample (solid line with UVES:  $\circ$ ; EMMI:  $\bullet$ ) and Galactic stars analysed with a blanketed version of FASTWIND (Urbaneja 2004; dash-dotted line with  $\triangle$ ). Also included are the WLR's from theoretical predictions based on Vink *et al.* (2001; dotted line) and unblanketed galactic results from Kudritzki *et al.* (1999; dashed line).

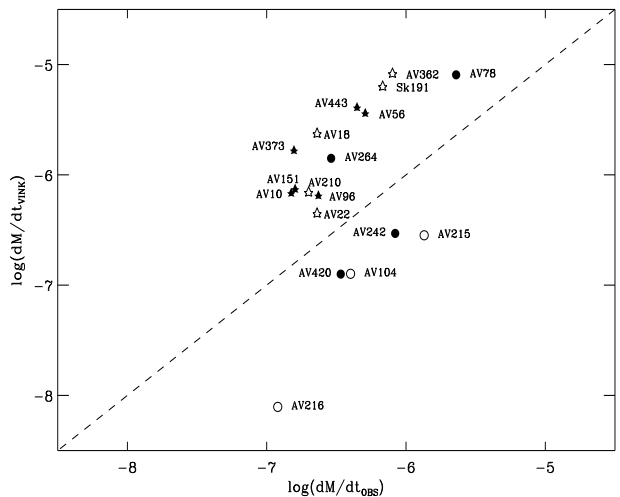


**Fig. 8.** Comparison of theoretical and observed mass-loss rates. Theoretical predictions are calculated using the metallicity dependent mass-loss recipes of Vink *et al.* (2001) for  $Z = 0.2 Z_{\odot}$ . The circles (UVES:  $\circ$ ; EMMI:  $\bullet$ ) represent the SMC early B-type supergiants, whilst the stars (UVES: open star; EMMI:  $\star$ ) represent the mid B-type supergiants.

ical prediction for a dependence of radiative driven winds on metallicity.

In Paper 1 the mass-loss rates derived from the observational data were discussed in relation to theoretical predictions from Monte-Carlo simulations (Vink *et al.* 2000, 2001). From

**Table 5.** The coefficients for the linear regression fits to the observed and theoretical predictions (Vink et al. 2001; V01) of the WLR from the SMC supergiants in this sample (all). Coefficients describing the relationship determined from the 4 early B-type supergiants, omitting the giant AV216, are also given (sg). In addition the values describing the relationship of only the mid B-type stars with  $T_{\text{eff}}$  in the range 22.5 - 16 kK are given (only < B3). Included are the coefficients for the Galactic B-type supergiants analysed by Kudritzki *et al.* (1999; K99) and that determined from the early B-type supergiants analysed by Urbaneja (2004; U04).

Analysis	$\log(D_{\odot})$	x	$\alpha'$
Early B-type stars			
SMC This work (all)	$20.45 \pm 2.54$	$1.46 \pm 0.44$	$0.68 \pm 0.15$
SMC This work (sg)	$17.91 \pm 6.11$	$1.91 \pm 0.93$	$0.52 \pm 0.43$
Galactic K99	$21.24 \pm 1.38$	$1.34 \pm 0.25$	$0.75 \pm 0.15$
Galactic U04	21.72	1.31	0.76
SMC V01	16.67	2.03	0.49
Mid B-type stars			
SMC This work (all)	$18.39 \pm 2.57$	$1.72 \pm 0.44$	$0.58 \pm 0.16$
SMC This work (only < B3)	$17.45 \pm 3.14$	$1.87 \pm 0.53$	$0.53 \pm 0.16$
Galactic K99	$17.07 \pm 1.05$	$1.95 \pm 0.20$	$0.51 \pm 0.05$
SMC V01	18.33	1.87	0.53

the analysis of the UVES data, a discrepancy was found between the observed mass-loss rates and theory; the theoretical predictions were lower for the early B and higher for the mid B-type stars by a factor of 5 and 7, respectively. A comparison of the entire sample of observed mass-loss rates with the theoretical predictions of Vink *et al.* (2001) for a metallicity of  $Z=0.004$  ( $0.2 Z_{\odot}$ ) is illustrated in Fig. 8. It is immediately evident from this plot that the behaviour of the EMMI sample is similar to that of the UVES dataset; the theoretical mass-loss rates of the early-type stars are under estimated and those of the cooler stars are over estimated in relation to the observed values (Note that the momentum driving the winds of AV78 and AV264 appear to follow the same pattern as the mid B-type stars). The Vink *et al.* (2000) formula also over estimates mass-loss rates for the Galactic mid B-type supergiants analysed by Kudritzki *et al.* (1999; this is illustrated in Fig 10 of Vink *et al.* 2000). It was shown by Vink *et al.* that  $\dot{M}$  derived from radio observations by Scuderi *et al.* (1998) appeared to be in agreement with the predictions for mid B-type supergiants. These two studies, also agreed with  $\dot{M}$  estimates from  $H_{\alpha}$  lines in pure emission but not with those derived with P-Cygni or absorption profiles. In the complete SMC sample considered here, seven out of thirteen mid B-type stars display pure emission and they do not appear to have systematically higher mass-loss rates than those derived from P-Cygni or absorption profiles. Therefore, the discrepancy between the Vink predictions and the observational results presented here does not appear to be a consequence of the  $H_{\alpha}$  profile.

This discrepancy with the theoretical predictions naturally results in a similar discrepancy in the wind-momenta. Adopting the predicted mass-loss rates and observed terminal velocities of the stars, the wind-momenta were determined. Fig 9 illustrates the significant difference between the linear regression fits to the observed and theoretical wind-momenta. The coefficients for the theoretical predictions are included in Table 5. An important point to note is that while the observed wind-

momenta for the early-type objects are higher than the mid B-type objects the opposite behaviour is predicted from the theoretical relationships (*i.e.* the mid B-type stars are predicted to have greater wind-momenta than their hotter counterparts). This is a substantial disagreement between the observational and theoretical results which may arise from the assumptions in either the model atmosphere analysis or the theoretical study of Vink *et al.* (2001). As discussed in Paper 1, the consideration of clumping in the wind can reduce the derived mass-loss rates and this would move the observational results of the early B-type objects into better agreement with the theoretical predictions. In contrast, clumping will increase the discrepancy with the mid B-type stars. Whilst a simple form of clumping can now be included in the unified model atmosphere codes such as CMFGEN and FASTWIND, invoking such processes is still largely speculative without knowledge of the clumping in the wind along our line of sight. In addition one must be aware of the variability in the winds of massive stars which time series optical (e.g.  $H_{\alpha}$  profile) and UV (e.g. P-Cygni lines) observations of galactic objects have revealed in recent years (for example Prinja, Massa & Fullerton 2002; Kaufer, Prinja & Stahl 2002; Morel *et al.* 2003; Prinja *et al.* 2004). Whilst the variability in the  $H_{\alpha}$  profiles of some of these Galactic objects may correspond to considerable changes in the properties of the winds, without further observations of the SMC objects we cannot investigate the extent of their variability (if any) and the subsequent affect on the derived wind parameters.

The theoretical predictions for the SMC objects give 0.49 and 0.53 as the value of the exponent  $\alpha'$  for early and mid B-type stars, respectively. This steeper relationship, in comparison to observations, is evident from Fig 9. The observed value of  $\alpha'$  has an important impact on stellar evolution calculations where it is used to describe mass-loss rates as a function of rotation. The smaller this factor the greater the mass-loss rate becomes at a given rotational velocity and position on the HR diagram. Thus,  $\alpha'$  has an influence on both the stellar life-

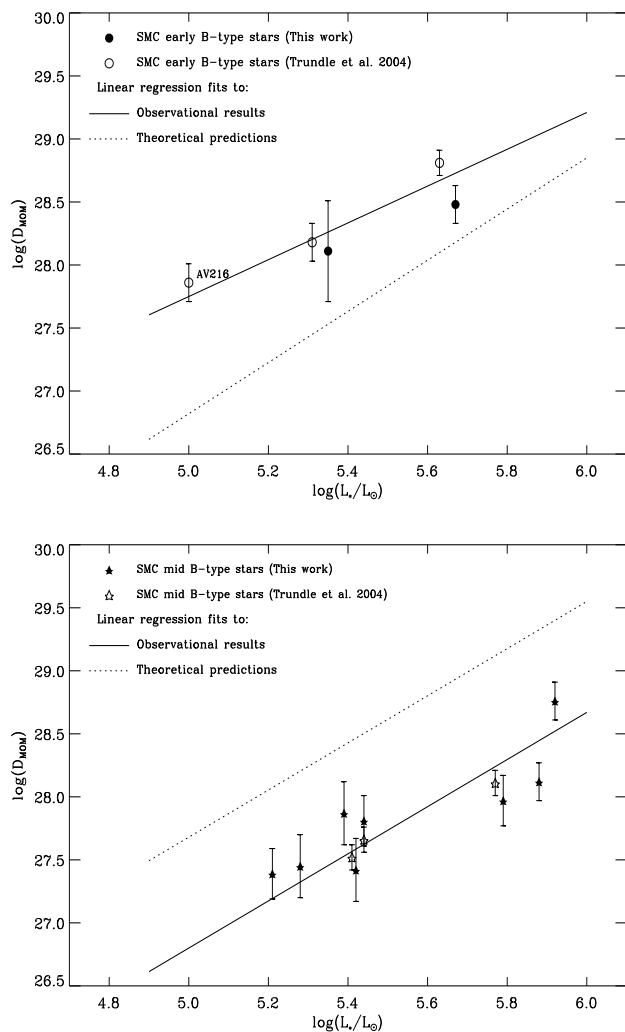


**Fig. 9.** Comparison of theoretical and observational wind momenta for B-type supergiants in the SMC. In the upper panel the observational result for the early B-type supergiants (UVES:  $\circ$ ; EMMI:  $\bullet$ ) from this work are considered. Included are the linear regression fits to the observational results (—; all) and the predicted wind-momenta of Vink *et al.* (2001;  $\cdots$ ). In the lower panel the observational result for the mid B-type supergiants (UVES: open star; EMMI:  $\star$ ) from this work are plotted together with the linear regression fits from the observational (only  $< B3$ ) and theoretical results. The error bars represent the uncertainty in deriving the wind momentum.

times and element yields. In the Maeder & Meynet (2001) code this exponent is assumed to be 0.66, which within the errors agrees well with those found from the current sample of stars. Nevertheless the large discrepancy between the mass-loss rates of the mid B-type stars is of concern. Since the large values predicted by Vink *et al.* (2001) would produce a rapid spin down as the star evolves beyond the main-sequence, which would not be predicted by evolution models if the observed results were invoked in the code. Furthermore  $\alpha'$  is important for the accu-

racy of the distances obtained from the WLR, since the distance derived is dependent on a precise determination of the luminosity. The steeper the WLR and hence smaller  $\alpha'$  the more accurately the luminosity of an object can be determined from its derived wind-momenta and subsequently the more useful the WLR technique is as a distance estimator.

## 6. Conclusions

In summary, a complete unified model atmosphere analysis has been completed for a further ten B-type supergiants in the SMC. By incorporating the eight stars analysed in paper 1, this sample of 18 objects has been considered in terms of the properties of their stellar winds and massive star evolution.

The nitrogen abundances in this dataset provide ample evidence of enhancement in the stellar photosphere. Incorporating the nitrogen abundances available in the literature for O-type stars and BA-type supergiants, it was shown that the majority of these have significantly enhanced nitrogen, with an average of 7.5 dex (*i.e.* close to solar abundance). This degree of nitrogen enrichment can be reproduced by stellar evolution models with initial rotational velocities of  $300 \text{ km s}^{-1}$  (Maeder & Meynet 2001). However, the high rotational velocities these models predict at the end of the main-sequence do not appear to be consistent with the observed projected rotational velocities.

A calibration of the wind-momenta as a function of luminosity for the B-type supergiants was considered, taking a step closer to the use of the WLR relationship as a distance indicator. The SMC relationships are inconsistent with the Vink *et al.* (2001) predictions, which for both the early and mid B-type objects are steeper. A comparison with two galactic early B-type stars analysed by Urbaneja (2004), revealed clear evidence for the metallicity dependence of radiatively driven winds.

Despite this, the spread in luminosity and temperature ranges possible for a given spectral type requires more extensive samples to disentangle the behaviour of momenta with these properties. In the future it is attractive to use larger samples to tie down this behaviour and determine  $\alpha'$ ; an important factor for stellar evolution codes.

## Acknowledgements

CT is grateful to the Department of Higher and Further Education, Training and Employment for Northern Ireland (DEFHTE) and the Dunville Scholarships fund for their financial support. DJL acknowledges funding from the UK Particle Physics and Astronomy Research Council (PPARC under the grant PPA/G/S/2001/00131. We would like to thank Joachim Puls and Robert Ryans for their continuous support with FASTWIND and TLUSTY, respectively. We are also grateful to Miguel Urbaneja for providing the galactic supergiant results and the referee, Alex Fullerton, for his useful comments.

## References

- Azzopardi, M., & Vigneau, J. 1982, A&AS, 50, 291
- Bouret, J.-C., Lanz, T., Hillier, D.J., Heap, S.R., Hubeny, I., Lennon, D.J., Smith, L.J., & Evans, C.J. 2003, ApJ, 595, 1182

- Crowther, P.A., Hillier, D.J., Evans, C.J., Fullerton, A.W., deMarco, O., & Willis, A.J. 2002, *ApJ*, 579, 774
- de Mello, D.F., Leitherer, C., & Heckman, T.M., 2000, *ApJ*, 530, 251
- Dufton, P.L., McErlean, N.D., Lennon, D.J., & Ryans, R.S.I. 2000, *A&A*, 353, 311
- Evans, C.J., Lennon, D.J., Trundle, C., Heap, S.R., & Lindler, D.J. 2004, *ApJ*, 607, 451
- Evans, C.J., Crowther, P.A., Fullerton, A.W., & Hillier, D.J. 2004a, *ApJ*, 610, 1021
- Fitzpatrick, E.L., & Bohannan, B. 1993, *ApJ*, 404, 734
- Fitzpatrick, E.L., & Garmany, C.D. 1990, *ApJ*, 363, 119
- Fullerton, A.W. et al., 2005 In *ASP Conf Ser. Astrophysics in the Far Ultraviolet*, eds Sonneborn, Moos, Andersson.
- Garmany, C.D., Conti, P.S., & Massey, P. 1987, *AJ*, 93, 1070
- Gies, D.R., & Lambert, D.L. 1992, *ApJ*, 387, 673
- Grebel, E.K., & Richtler, T. 1992, *A&A*, 253, 359
- Harries, T.J., Hilditch, R.W., & Howarth, I.D. 2003, *MNRAS*, 339, 157
- Haser, S.M. 1995, PhD Thesis, Universitäts-Sternwarte
- Herrero, A., Puls, J., & Najarro, F. 2002, *A&A*, 396, 949
- Hill, V. 1999, *A&A*, 345, 430
- Hillier, D.J., Lanz, T., Heap, S.R., Hubeny, I., Smith, L.J., Evans, C.J., Lennon, D.J., & Bouret, J.C. 2003, *ApJ*, 588, 1039
- Howarth, I.D., Murray, J., Mills, D., & Berry, D.S. 2003, *Starlink User Note* 50
- Kaufert, A., Prinja, R.K. & Stahl, O. 2002, *A&A*, 382, 1032
- Kubát J., Puls, J., & Pauldrach, A.W.A. 1999, *A&A*, 341, 587
- Kudritzki, R.-P., Lennon, D.J., & Puls, J. 1995, in *Science with the VLT*, eds. J.R. Walsh & I.J. Danziger, (Heidelberg: Springer), 246
- Kudritzki, R.-P., Puls, J., Lennon, D.J., Venn, K.A., Reetz, J., Najarro, F., McCarthy, J.K., & Herrero, A. 1999, *A&A*, 350, 970
- Kudritzki, R.-P., & Puls, J. 2000, *ARA&A*, 38, 613
- Kurt, C.M., Dufour, R.J., Garnett, D.R., Skillman, E.D., Mathis, J.S., Peimbert, M., Torres-Peimbert, S., & Ruiz, M.-T. 1999, *ApJ*, 518, 246
- Lamers, H.J.G.L.M., Snow, T.P., & Lindholm, D.M. 1995, *ApJ*, 455, 269
- Leitherer, C., Leão, J.R.S. 1999, *ApJS*, 123, 3
- Lennon, D.J., Kudritzki, R.-P., Becker, S.T., Butler, K., Eber, F., Groth, H.G., & Kunze, D. 1991, *A&A*, 252, 498
- Lennon, D.J., Dufton, P.L., Mazzali, P.A., Pasian, F., & Marconi, G. 1996, *A&A*, 314, 243
- Lennon, D.J. 1997, *A&A*, 317, 87
- Lennon, D.J., Dufton, P.L., & Crowley, C. 2003, *A&A*, 398, 455
- Meynet, A., & Maeder, G. 2000, *A&A*, 361, 159
- Maeder, A., & Meynet, G. 2001, *A&A*, 373, 555
- Markova, N., Puls, J., Repolust, T., & Markov, H. 2004, *A&A*, 413, 693
- Massey, P. 2002, *ApJS*, 141, 81
- McErlean, N.D., Lennon, D.J., & Dufton, P.L. 1999, *A&A*, 349, 553
- McGee, R.X., & Newton, L.M. 1981, *PASP*, 4, 189
- Morel, T. et al., 2003, *MNRAS*, 351, 552
- Pettini, M., Steidel, C.C., Adelberger, K.L., Dickinson, M., & Giavalisco, M. 2000, *ApJ*, 528, 96
- Prinja, R.K., et al. 2004, *A&A*, 418, 727
- Puls, J., et al. 1996, *A&A*, 305, 171
- Puls, J., Springmann, U., & Lennon, M. 2000, *A&AS*, 141, 23
- Puls, J., Urbaneja, M.A., Venero, R., & et al. 2005, *A&A*, accepted
- Repolust, T., Puls, J., & Herrero, A. 2004, *A&A*, 415, 349
- Rolleston, W.R.J., Venn, K., Tolstoy, E., & Dufton, P.L. 2003, *A&A*, 400, 21
- Santolaya-Rey, A.E., Puls, J., & Herrero, A. 1997, *A&A*, 323, 488
- Sanduleak, N. 1968, *AJ*, 73, 246
- Scuderi, S., Panagia, N., Stranghellini, C. & et al. 1998, *A&A*, 332, 231
- Trundle, C., Lennon, D.J., Puls, J., & Dufton, P.L. 2004, *A&A*, 417, 217
- Urbaneja, M.A. 2004, PhD Thesis, University of La Laguna
- Venn, K.A. 1999, *ApJ*, 518, 405
- Venn, K.A., & Przybilla, N. 2003, in *ASP Conf. Ser. 304, CNO in the Universe*, eds. Charbonnel C., Schaerer, D., Meynet, G., (ASP, San Francisco), in press (astro-ph/0212258)
- Vink, J.S., deKoter, A., & Lamers, H.J.G.L.M. 2000, *A&A*, 362, 295
- Vink, J.S., deKoter, A., & Lamers, H.J.G.L.M. 2001, *A&A*, 369, 574
- Welty, D.E., Frisch, P.C., Sonneborn, G., & York, D.G. 1999, *ApJ*, 512, 636